Influence of Flank Face Structuring on Cooling, Tool Lifetime and Borehole Quality When Drilling Inconel 718: Physical Simulations and Experimental Validation

Daniel Müller
Institute for Manufacturing Technology and Production Systems,
Technische Universität Kaiserslautern, Germany

Benjamin Kirsch
Institute for Manufacturing Technology and Production Systems,
Technische Universität Kaiserslautern, Germany

Jan C. Aurich
Institute for Manufacturing Technology and Production Systems,
Technische Universität Kaiserslautern, Germany

Abstract

When drilling difficult-to-cut materials such as Inconel 718, the drills are exposed to high thermo-mechanical loads. Due to the low thermal conductivity of the workpiece material, a large amount of the generated heat has to be dissipated by the metal working fluid (MWF). However, the cutting zone is located inside the workpiece, which makes it challenging to provide sufficient MWF to the cutting zone. To solve this, drills with internal cooling channels are commonly used. In this work, the influence of differently structured flank faces on cooling efficiency, tool life, process forces and borehole quality is investigated. The influence of the structures on the cooling was investigated by Computational-Fluid-Dynamics (CFD) simulations. These simulations allow a detailed analysis of the flow conditions inside the borehole and showed that the structuring improved flow conditions, especially near the thermally highly loaded main cutting edge. The improved flow conditions resulted in an extension of the tool life by up to 22 % compared to unstructured drills in experimental investigations.

2012 ACM Subject Classification Applied computing → Physical sciences and engineering

Keywords and phrases drilling, cooling, CFD

Digital Object Identifier 10.4230/OASIcs.iPMVM.2020.7

Funding The investigations presented here partly result from the research project IGF 19154N of the German Machine Tool Builders' Association (VDW). It was funded within the program for industrial collective research (IGF) by the Federal Ministry of Economics and Technology (BMWi) via the German Federation of Industrial Research Associations (AiF). This research was also partly funded by the Deutsche Forschungsgemeinschaft (DFG, German Research Foundation) – 252408385 – IRTG 2057.

1 Introduction

The nickel-based alloy Inconel 718 is one of the most widely used superalloys. It was developed for applications in aerospace turbines, but is also used in the automotive and chemical industries, due to its excellent material properties [4]. Inconel 718 provides superior mechanical properties such as high tensile, fatigue and fracture strength even at temperatures above 700°C. During machining, these material properties as well as the tendency to work hardening lead to high thermal and mechanical loads on the tools and consequently to a low productivity and a limited tool life [4, 21].

2nd International Conference of the DFG International Research Training Group 2057 – Physical Modeling for Virtual Manufacturing (iPMVM 2020).
Editors: Christoph Garth, Jan C. Aurich, Barbara Linke, Ralf Müller, Bahram Ravani, Gunther Weber, and Benjamin Kirsch; Article No. 7; pp. 7:1–7:17

OpenAccess Series in Informatics
Schloss Dagstuhl – Leibniz-Zentrum für Informatik, Dagstuhl Publishing, Germany

Drilling is one of the oldest and most important machining processes. With regard to the process conditions, the process has some specific characteristics: an unfavorable heat distribution in the cutting zone, a cutting speed that drops to zero towards the axis of rotation, the rubbing of the chips as well as the rubbing of the margin against the surface of the borehole as well as a difficult evacuation of the chips. Due to the unfavorable heat distribution in the cutting zone and the nearly complete conversion of the mechanical energy applied for cutting into heat, the tools are exposed to high thermal loads [10]. As the strength of carbides decreases with increasing temperature, the wear resistance also decreases with increasing temperature [10]. To counteract this, metalworking fluids (MWF) are used to reduce the thermal load and consequently the wear of the drill. Besides the increase of the tool life, an efficient supply of the cooling lubricant to the cutting zone also leads to an improved machining quality [10, 20].

The removal of chips through the chip flutes of the drills and the position of the cutting zone inside the workpiece make an external coolant supply difficult. For this reason, in industry internal coolant supply is used, especially for deep bores (length/diameter > 3). The MWF is supplied via channels inside the tool. The outlet positions of the helical channels are on the flank faces of the drill and lead to an indirect cooling of the cutting zone. This results in improved cooling of the tool and the workpiece. Furthermore, the chip removal is supported and the friction between tool and chips is reduced [10]. The productivity of drills can be increased by a more efficient cooling lubrication by means of optimized internal cooling [5]. To improve internal cooling conditions, different design elements can be used. Previous investigations on internal MWF supply have focused on the flow behaviour within the cooling channel and the flute [9, 17]. Oezkaya et al. [15] analyzed the influence of the cooling channel diameter and the supply pressure on the cooling efficiency. Their findings showed that especially a higher supply pressure improves the cooling. Also, the integration of structures into the flank face near the main cutting edge can lead to improved cooling lubrication [3, 7, 16]. By adding grooves in the flank face, Guo et al. were able to minimize the feed forces and wear [7]. Beer et al. were able to achieve tool life increases up to 50 % by adding a groove-shaped structure in the first flank face. Furthermore, the structuring led to an improved borehole and surface quality [3].

In our previous works, the influence of the cooling channel outlet position at the flank face was investigated by numerical flow simulations and experiments. It was shown that cooling channel outlets near the main cutting edge lead to an improved cooling [5, 6]. The work in [14] and [13] focused on the influence of the second clearance angle, the number of cooling channels as well as the cooling channel diameter with respect to the thermal load of the tools. An enlargement of the cooling channel diameter and a decrease of the second clearance angle led to better cooling [13], whereas an increase in the number of cooling channels resulted in a deterioration of the cooling. Simulative investigations in [12] showed that the integration of structures in the first flank face can improve the flow conditions and thus also the efficiency of the cooling. Furthermore, it was shown that the influence of the structural shape on the cooling is more significant than the influence of the increased surface and the increased flow volume [12].

In this paper, an approach for the simulative investigation of internally cooled drills is presented and the influence of structured flank faces on the cooling of the drill, tool life, process forces and borehole quality have been investigated.

2 Experimental design

2.1 Machining Setup

Drilling was performed on a 5-axis machining centre (DMU 70 eVolution[1]) with the experimental setup shown in Figure 1a. Blind holes with a depth d_h of 24 mm were drilled at a cutting speed v_c of 20 m/min and a feed rate f of 0.09 mm/rev. A constant MWF volume flow rate $\dot{V}$ of 1 l/min (emulsion, 6 %) was chosen. The experiments were carried out on Inconel 718. The tools used were uncoated cemented carbide (K40UF: 10 % CO and 90 % WC) twist drills with a drill diameter d of 8 mm. All drills had a point angle σ of 140°, a twist angle ϵ of 30°, a first clearance angle α_1 of 10° and a second clearance angle α_2 of 25°. The distance from the center of the cooling channels to the center of the drill r_c was 3.8 mm, and the cooling channel diameter d_c was 1 mm. The variations of the structuring can be seen in Figure 1b. All structures had a spacing of 150 µm to the main cutting edge, a depth of 55 µm and were created by laser.

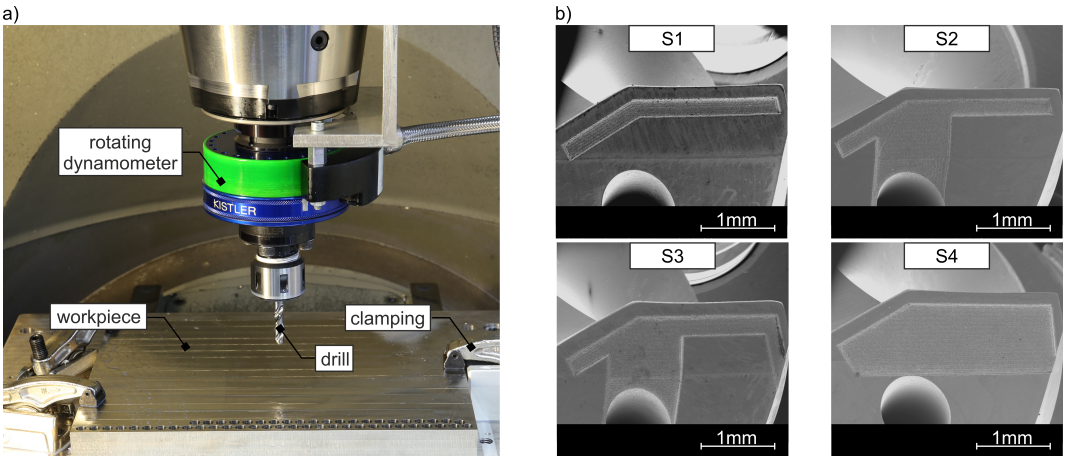

Figure 1 a) Experimental setup b) Structured drills.

The structures S1 to S3 are groove-shaped cavities along the cutting edge. The shape of the grooves was adapted to the shape of the main cutting edge to improve the flow conditions in this area. Based on S1, a connection between the cooling channel and the structure was implemented for S2 - S3. For S3 an additional slot was added near the cutting edge corner. The intention of the additional slots is to improve the fluid flow into the grooves. For structure S4, almost the entire area of the first flank face and parts of the second flank face were lowered.

2.2 Characterization methods

The forces in x-, y- and z-direction and the torque during drilling were measured using a rotating dynamometer (Kistler 9123 C[1]) with a sampling rate of 2 kHz. From each drill variant, two drills were used. To determine the forces, the torque and the borehole quality, measurements were taken at each data point over 3 consecutive boreholes per tool. Averaging was therefore carried out over 6 measurements.

The maximum width of flank wear land depending on the drilling path was determined through macroscopic images. The maximum width of flank wear land was evaluated at all four cutting edges per variation (2 tools for each variant) and the values were averaged. The

uncertainty of the measurement results is given by the average standard deviation $\overline{\sigma}$. To obtain the average standard deviation, the standard deviations were first calculated at every data point from the four measurements of each drill variant. Then, the arithmetic mean of all standard deviations for the respective variable was calculated.

The borehole quality was determined by evaluating the diameter, the concentricity and the roundness of the boreholes with a 3D coordinate measuring device (TESA Micro-Hite 3D dcc[1]). Nine measurement planes were placed in the boreholes every 2 mm. For each measurement plane, nine equally distributed measurement points were used. The first measurement plane of the respective borehole served as reference plane for the calculation of the concentricity. In order to consider the influence of the drill diameter on the diameter of the borehole, the borehole diameters were normalized according to:

$$d_{borehole} = \frac{\overline{d}_{borehole}}{d_{drill}} d_{drill}^{ideal} \tag{1}$$

where $\overline{d}_{borehole}$ is the measured borehole diameter, d_{drill} is the measured drill diameter and d_{drill}^{ideal} is the ideal drill diameter (8.0 mm). The surface roughness of the boreholes was determined by a stylus instrument (MarSurf XR20 GD120[1]) according to DIN EN ISO 4288 both at the entrance and the end of the borehole by means of three measurements over the circumference of the borehole. The surface roughness was specified via the average surface roughness R_z and the maximum surface roughness R_{max}.

The static pressure of the MWF within the collet before entering the drill was measured with a pressure sensor (Entran EPX-N01-70B[1]).

3 Numerical Simulation

Computational Fluid Dynamics (CFD) simulations have been proved to be a useful tool to analyze and visualize the flow conditions of internally cooled drills [12, 15]. The approach for such simulations is divided into the following five steps: Creation of the geometry (CAD model), discretization of the CAD model (meshing), definition of the boundary conditions, iterative computation and evaluation of the simulation results. The simulations presented here were carried out with Ansys CFX[1].

3.1 CFD fundamentals

The basic equations in numerical flow computations are the conservation laws of mass, momentum and energy. These equations describe all flows of Newtonian fluids. However, the computation workload, especially for turbulent flows, can become very high, due to the non-linearity. Therefore, most CFD programs are based on the Reynolds-averaged Navier-Stokes equations. These equations represent the physics with sufficient accuracy and acceptable computing time. Small turbulences are not resolved, but modelled by turbulence models. In addition to a suitable turbulence model, the boundary conditions at the inlet and outlet must also be selected carefully [8].

3.2 Drill geometry and fluid volume

The basis for the simulations were the CAD models of the examined drills. A scan of the reference tool was used to create a parameterizable CAD model of the drill geometry by reverse engineering. By scanning the tool, the exact geometry of the drill can be used within the simulations, which allows a comparison of the simulated findings with the experimental

results. To reduce the computational time, only the drill tip with a length of 10 mm (model reduction) was considered within the simulations. The structures were implemented in accordance with the real tools. Besides the drills, the respective complementary fluid volumes, which represent the flow area within the simulation, were also created by means of a Boolean operation.

3.3 Mesh

The quality of the mesh is fundamental for the accuracy, the reliability and computing time of the simulation [8]. A high-quality mesh implies refinements in areas of interest, a good aspect ratio, and only as few cells as necessary. Due to the complex geometry of the tool and the fluid volume, unstructured meshes of tetrahedron elements with a size of 2.0 µm up to 400 µm were used. The mesh of the fluid volume was refined (2-7 µm) in particular near the main cutting edge, at the cooling channels, at the structures and in the area of the heat input. Special attention was given to the area of the fluid volume near the main cutting edge between the flank face and the bottom of the bore hole. Due to the narrow space in this area, an inflation layer was applied in addition to the refinement (Figure 2).

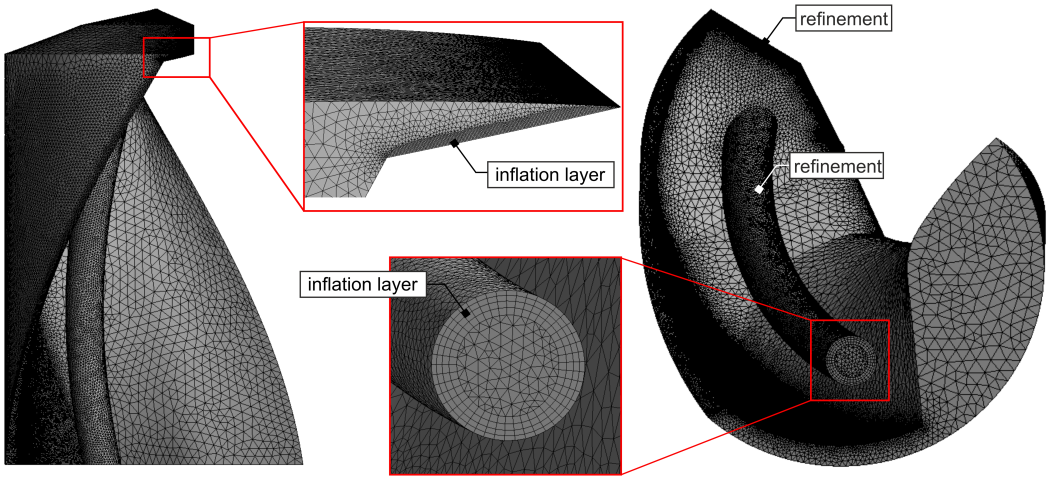

Figure 2 Mesh of the fluid volume.

3.4 Transferred boundary condition

Due to the model reduction described in Section 3.2, the results could differ from those of a complete model. However, the calculation of a complete model would be very time-consuming. To exclude possible discrepancies a second simulation model was used to generate a transferred boundary condition [2]. For this purpose, a model was built which calculates the flow conditions of the complete model, whereby e.g. the drill geometry and thermal effects are neglected for reasons of computing time. The flow conditions at different positions of the model can then be exported and used as a boundary conditions (transferred boundary condition) for all the simulations with the reduced models. As a result, all simulations can be carried out with a better accuracy and an overall reduced computing time. The model used maps the geometry of the cooling channels of the drill and the interior of the chuck up to the location where the fluid pressure is measured (Figure 3a). At the inlet of the model, the determined pressure (3.3 bar) was used as the boundary condition (total pressure) and at the

outlet the corresponding volume flow rate (1 l/min). An unstructured mesh of tetrahedron elements with a size of 5.0 µm up to 600 µm was used. The cooling channels were refined and an inflation layer was applied (Figure 3b). To model the turbulences, the κ-ω-SST (Shear Stress Model) was used [5, 15]. This turbulence model combines the advantages of the most frequently used turbulence models κ-ω and κ-ε. As a result, the turbulences near the wall as well as far from the wall are represented most realistically [19]. The convergence criterion of the simulation was defined to be 10^{-5}.

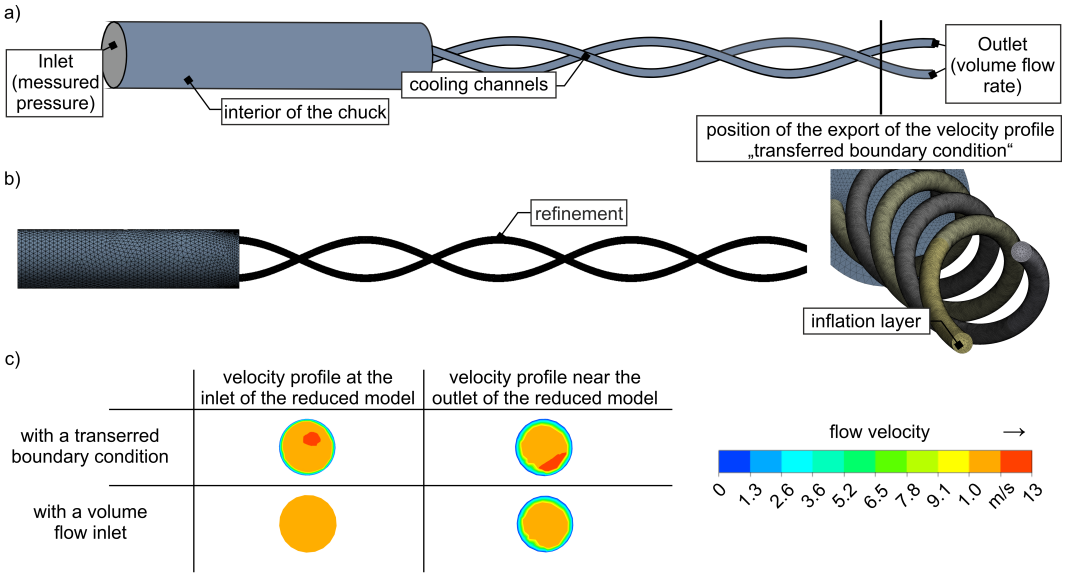

Figure 3 a) Model to simulate the flow conditions inside the cooling channels b) Mesh of the model c) Influence of the inlet boundary condition on the flow inside the cooling channel.

Figure 3c shows the flow profiles of the reduced model at the inlet of the cooling channel and near to the outlet of the cooling channel. The upper line contains the resulting flow profiles when using a transferred boundary condition, the lower line shows the profiles when using a volume flow inlet. Applying the transferred boundary condition, a completely defined flow profile is obtained at the inlet, whereas using a volume flow inlet results in a constant flow velocity over the inlet. Even near the cooling channel outlet, differences in the flow conditions are still apparent, which could influence the results regarding the cooling of the tool.

In order to transfer the resulting flow conditions of the complete model to the reduced model, the velocity profile was exported from the complete model at the position of the inlet of the reduced model and then used in the reduced model as the inlet boundary condition.

3.5 Boundary conditions

The κ-ω-SST (Shear Stress Model) was used to model the turbulence. The boundary condition at the inlet was the transferred velocity profile. An opening with ambient pressure was defined as the boundary condition at the flute. A rotational speed of 796 min^{-1} was applied to the drill and the fluid volume, which corresponds to a cutting speed of 20 m/min. The convergence criterion was 10^{-5}. In order to consider the heat input into the drill during the cutting process, an approach from Lazoglu et al [11] to simulate temperature fields on the drilling tool was adopted.

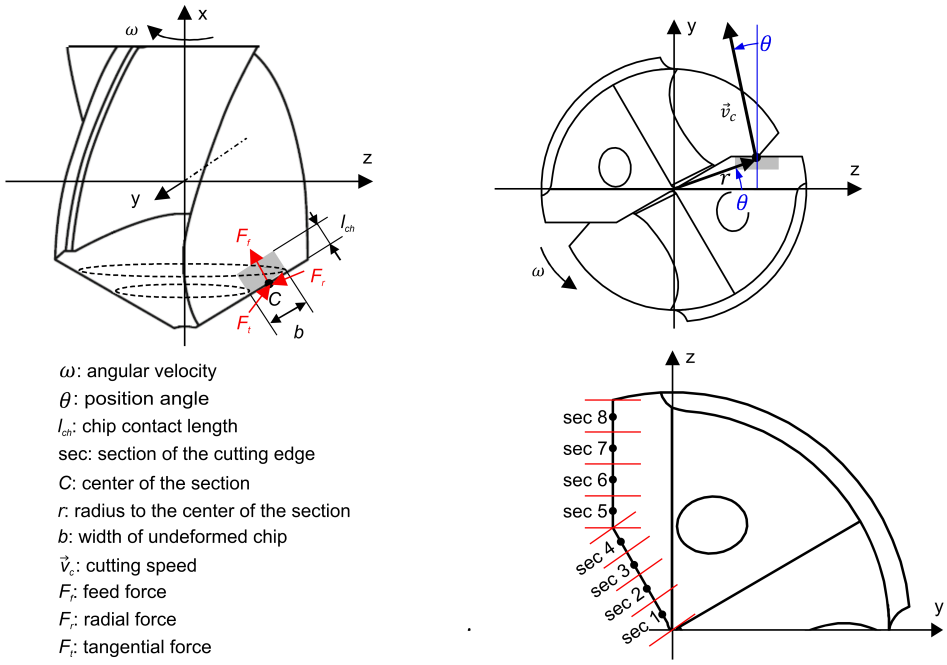

Figure 4 Discretization of the cross-section of the undeformed chip.

Thereby the heat input is estimated via the frictional power within the cutting process. For this purpose, the cutting forces along the main cutting edge are calculated using the discretized orthogonal to oblique transformation model as described by Altintas [1].The cross-section of the undeformed chip was discretized into eight sections (sec) according to Figure 4 and the discrete force components along the tangential F_t, feed F_f and radial F_r direction as well as the resultant cutting force F_{res} were calculated in every section according to the equations 2-5 [1]:

$$F_t = \frac{\tau_s bh[cos(\theta_n) + tan(\theta_i)tan(i)]}{[cos(\theta_n + \phi_n)cos(\phi_i) + tan(\theta_i)sin(\phi_i)]sin(\phi_n)} \tag{2}$$

$$F_f = \frac{\tau_s bhsin(\theta_n)}{[cos(\theta_n + \phi_n)cos(\phi_i) + tan(\theta_i)sin(\phi_i)]cos(i)sin(\phi_n)} \tag{3}$$

$$F_r = \frac{\tau_s bh[tan(\theta_i) - cos(\theta_n)tan(i)]}{[cos(\theta_n + \phi_n)cos(\phi_i) + tan(\theta_i)sin(\phi_i)]sin(\phi_n)} \tag{4}$$

$$F_{res} = \sqrt{F_t^2 + F_f^2 + F_r^2} \tag{5}$$

The tool orthogonal rake angle γ_n and the inclination angle i were determined on the geometry model for each segment. The friction angle β_α was calculated using the chip compression ratio r_c. The chip compression ratio r_c is the ratio of the uncut chip thickness h over the deformed chip thickness h_c [1]. The deformed chip thickness was determined experimentally ($h_c = 0.06$ mm).

$$i = sin^{-1}(sin(\theta)\ sin(\frac{\sigma}{2})) \tag{6}$$

$$\beta_\alpha = 45° + \gamma_n - tan^{-1}(\frac{r_c sin(\gamma_n)}{1 - r_c sin(\gamma_n)}) \tag{7}$$

$$r_c = \frac{h}{h_c} \tag{8}$$

The chip flow angle η, oblique shear angle ϕ_i, normal shear angle ϕ_n and the direction of the resultant force vector (θ_i and θ_n) were determined for each segment according to the "maximum shear stress principle" (Figure 5) [1]. The convergence criterion for the computation of the angles was chosen to be 10^{-12}.

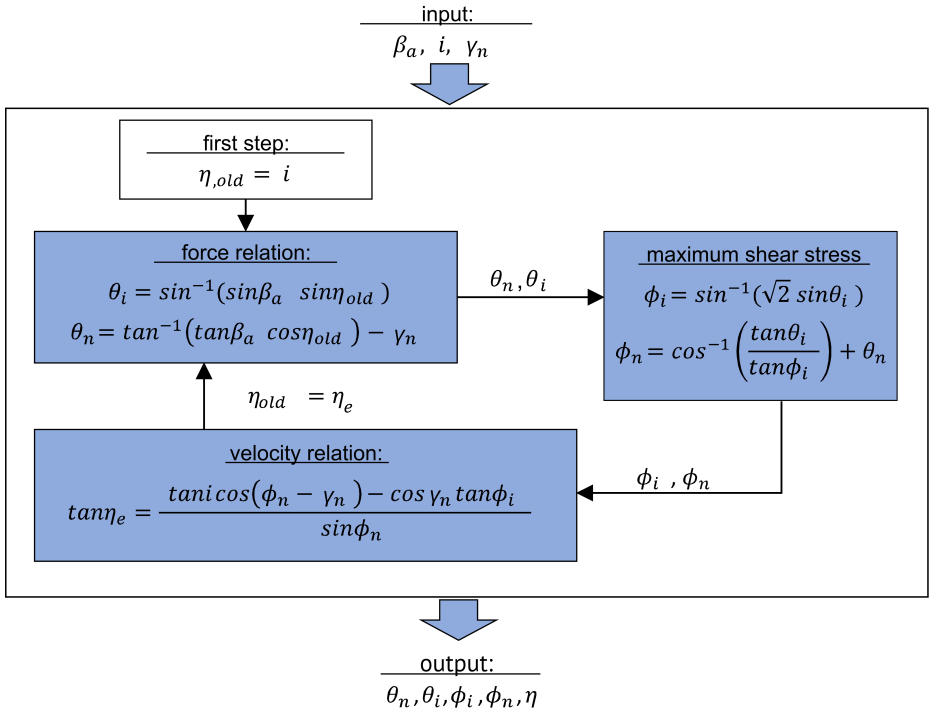

Figure 5 Calculation of the required angles according to the maximum shear stress principle.

The friction force F_{fr} in each segment can be determined using the friction angle β_α and the resulting cutting force F_{res} [1]:

$$F_{fr} = F_{res} sin(\beta_\alpha) \tag{9}$$

The resulting angles and forces along the main cutting edge are shown in Figure 6.

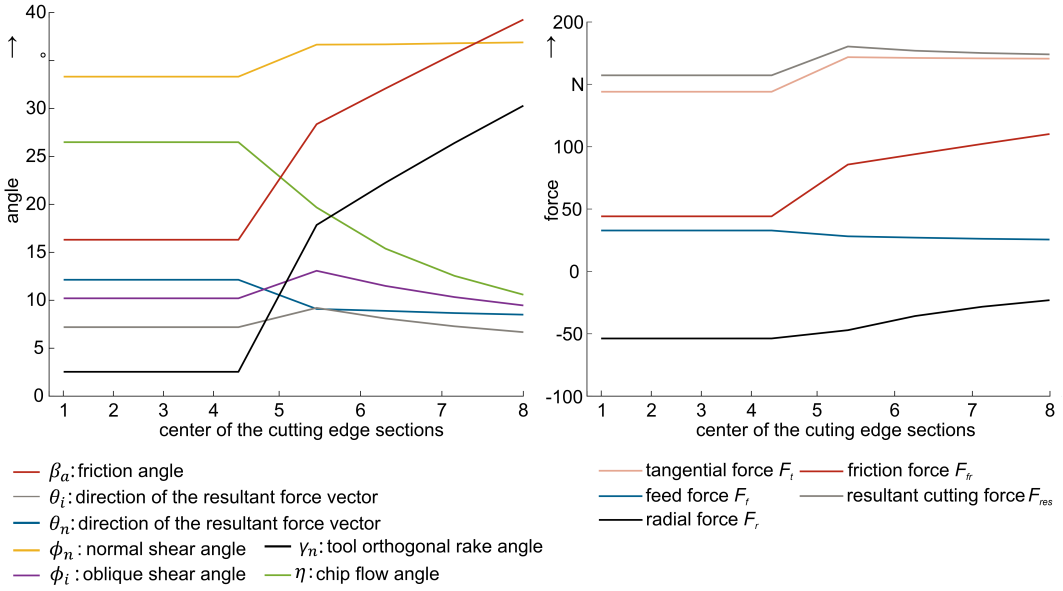

Figure 6 Calculated angles and forces along the main cutting edge.

The friction power P_{fr} is the product of the friction force F_{fr} and the chip velocity v_{ch}, given by [1]:

$$P_{fr} = F_{fr} v_{ch} \tag{10}$$

$$v_{ch} = \frac{v_c \sin(i) \sin(\Phi_n) \sec(\eta)}{\tan(\Phi_i) \cos(\gamma_n) + \sin(\Phi_n) \tan(\eta)} \tag{11}$$

The effective heat input P_{eff} into the drill for each section was obtained by including the heat partition coefficient λ [11]:

$$P_{eff} = \lambda P_{fr} \tag{12}$$

The heat partition coefficient λ was calculated corresponding to cutting speed v_{ch} of each section as reported in [18]:

$$\lambda = 1.17\ {v_c}^{-0.293} \tag{13}$$

The effective heat input was introduced at the rake face in the area of the chip contact. For this purpose, the effective heat flux density q_{eff} was calculated for each segment of the rake face from the effective power P_{eff} and the surface A of the respective element.

$$q_{eff} = \frac{P_{eff}}{A} \tag{14}$$

For the heat transfer between fluid and solid the conservative interface flux option was used at the Fluid-Solid interface and the Solid-Fluid interface. All remaining surfaces were defined as adiabatic. The cutting zone is cooled indirectly via the flank face. In order to calculate the heat distribution, the heat capacity, thermal conductivity and density of the cemented carbide and metalworking fluid were included in the simulation according to manufacturer's

specifications. The chip contact length l_{ch} along the main cutting edge was calculated for every section according to [1]:

$$l_{ch} = \frac{h \sec(\eta) \sin(\Phi_n + \theta_n)}{\sin(\Phi_n)[\cos(\gamma_n)\cos(\theta_n) - \sin(\gamma_n)\sin(\theta_n)]} \tag{15}$$

The calculated heat input for each section is shown in Figure 7a. The heat input increases in the direction of the cutting edge corner (Figure 7b). This results in particular from the increase of the cutting speed along the main cutting edge in the direction of the cutting edge corner.

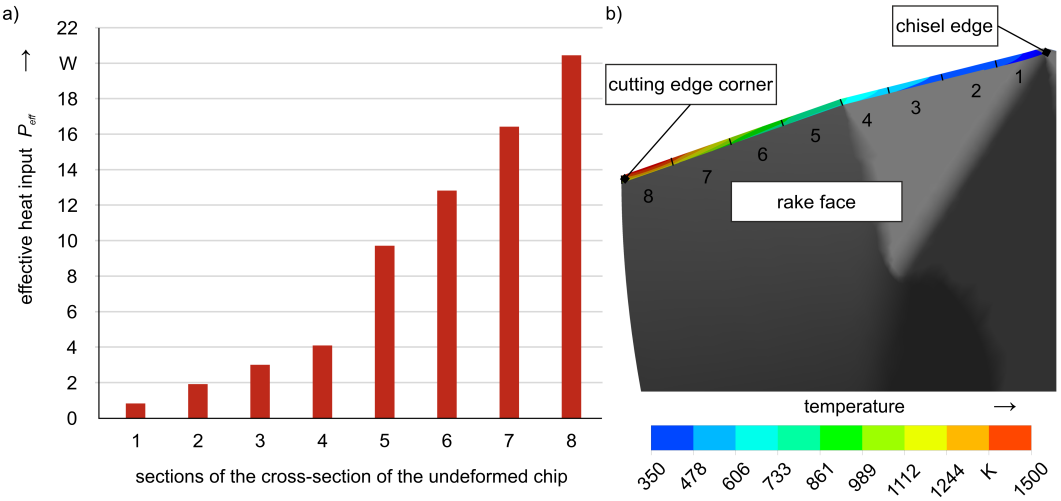

Figure 7 a) Effective heat input for every section b) Temperature distribution in the area of the chip contact length.

4 Results

4.1 Simulation

The flow velocities in the area of the first, second, and third flank face are shown as vectors in Figure 8. The vectors of the reference drill without structuring (ref.), show the highest flow velocities in the area of the second flank face. The flow velocities decrease in the area of the first flank face and in direction to the main cutting edge. Moreover, in some areas near the main cutting edge, dead zones can even be seen, i.e. areas with almost no flow velocity. This is in particular true in front of the cooling channel outlet and close to the cutting edge corner. By integrating the groove-shaped structures (S1 – S3) and the structure S4, the velocity can be increased in the area of the first flank face compared to the reference. The size of the dead zones can also be reduced, especially in front of the cooling channel outlet. In addition, the flow velocity is increased through the structuring in the area of the cutting edge corner. Especially the groove-shaped structures (S1 – S3) reduce the dead zones near the cutting edge corner. Comparing the groove-shaped structures (S1 - S3) with each other, there are no significant differences in flow distribution and flow velocities between S2 and S3. In the area of the additional slot between the cooling channel and the structure, S2 and S3 have slightly lower flow velocities than S1. Structure S4 shows the most even flow distribution in the area of the first flank face compared to the other drills. In particular, the dead zone in front of the cooling channel outlet is reduced compared to the reference, and also the dead zone close to the cutting edge corner is reduced.

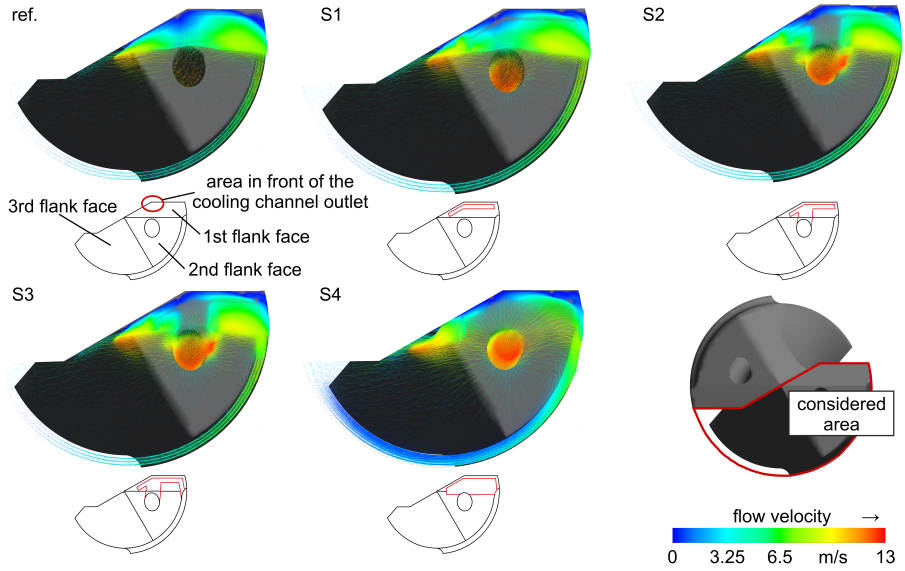

Figure 8 Resulting flow vectors at a volume flow rate of 1 l/min.

Previous investigations, dealing with the optimization of the cooling of internally cooled drills, have shown that an increase in the flow velocity near the main cutting edge and in the area of the first flank face lead to a reduction of the temperatures in the cutting wedge [3, 12, 16].

Figure 9 (left) shows the resulting temperatures in the area between the main cutting edge and the structures. The average temperature of the main cutting edge of all drills is given on the right hand side of Figure 9.

Compared to the reference, all structures cause a reduction in temperature, especially near the cutting edge corner. By integrating structure S1, the temperatures are reduced most significantly in the area of the cutting edge corner. In contrast to the reference drill, the average temperature of the main cutting edge is reduced by about 47 K. In comparison with the structure S1 and S3, structure S2 reduces the temperatures near the chisel edge most significantly, whereas the temperatures near the cutting edge corner are slightly higher compared to S1. Compared to the reference the average temperature of the main cutting edge is reduced by about 41 K. The temperature distribution of S3 is similar to that of S1, deviating only near the cutting edge corner with slightly higher temperatures. The average temperature of the main cutting edge compared to the reference is reduced by about 44 K for S3. The most significant reduction in the average temperature of the main cutting edge (54 K) compared to the reference is offered by structure S4. Furthermore, S4 has the lowest temperatures in front of the cooling channel outlet. However, higher temperatures occur near the cutting edge corner than for S1.

The combination of an increase in surface area and in fluid volume as well as overall improved flow conditions leads to an enhanced cooling of the drill. The described flow conditions above the first flank face are in-line with the resulting temperatures.

The resulting temperatures in the cutting wedge are shown on a plane 60 µm below the first flank face (Figure 10).

For all drill variants, the highest temperatures occur near the rake face and in the direction of the cutting edge corner. The reference drill (ref.) shows the highest temperatures of all drill variants on the entire plane. The groove-shaped structures as well as the structure S4

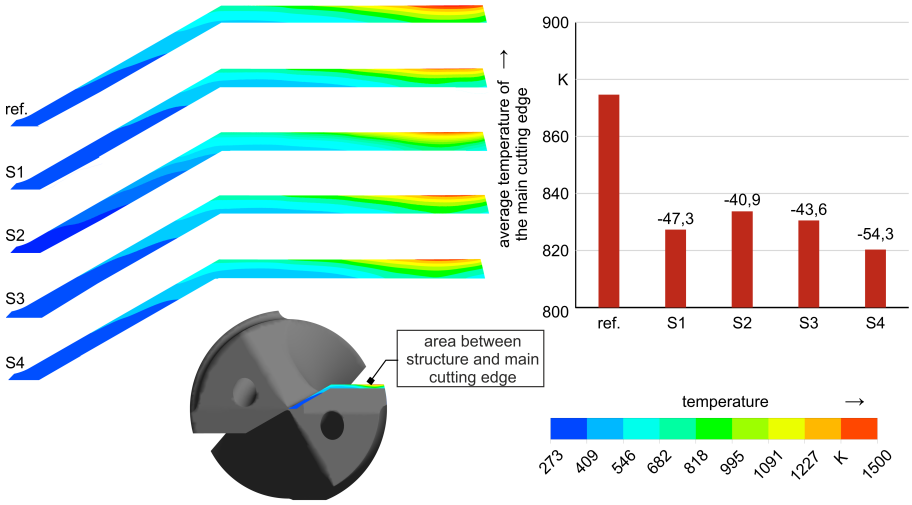

Figure 9 Resulting temperatures near the main cutting edge (left) and average temperature of the main cutting edge (right) at a volume flow rate of 1 l/min.

reduce the temperatures in particular near the rake face and in the area of the cutting edge corner. Structure S1 shows the lowest overall temperatures and leads to significantly lower temperatures near the cutting edge corner compared to the reference (ref.). S2, S3 and S4 have similar temperature distributions along the rake face.

4.2 Experiment

The results of the maximum width of flank wear land (VB_{max}) over the drilling path are shown in Figure 11. A degressive wear progress can be determined for all drill variants. Up to a drilling path of 0.3 m the maximum width of flank wear land increases strongly, thereafter the curve is characterized by a quasi-linear progress. The wear curves of the investigated drill variants start differing significantly after reaching a drilling path of 1.4 m. This is followed by a widening spread, where the structured drills (S1 - S4) show overall lower values of the maximum width of flank wear land in comparison to the reference drill (ref.) The most significant increase in tool life is caused by structure S1, with an improvement of about 21 % compared to the reference. Structures S2 and S3 lead to an increase in tool life of 11 % and 17 % respectively. S4 increases the tool life by 13 %. Since the same process conditions (feed rate, cutting speed, MWF flow rate and pressure) and the same drill geometry were used for all investigated drills, these longer tool lifetimes can only be attributed to the improved flow conditions resulting from the structuring.

The torques in the rotational axis and the forces in the feed direction in function of the wear condition and structuring are shown in Figure 12. An increase due to wear can be observed for all torque values. These increases compared to the unworn condition vary between 7 % to 10 %. For both wear conditions, no significant differences (max. 2 %) in torque can be identified in dependence of the structures. Furthermore, no systematic and no significant influence (max. 3 %) of the wear condition on the feed force can be identified. Also, no significant influence of the structuring and structural shape on the feed force (max. 4 %) can be detected.

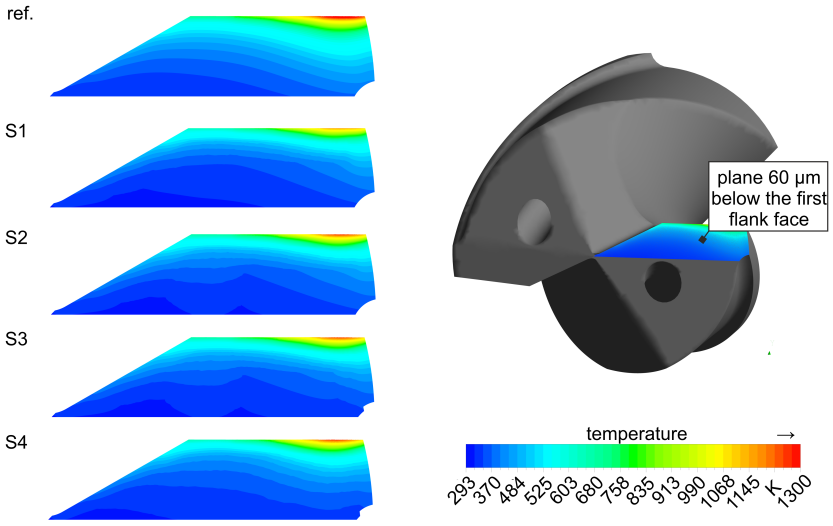

Figure 10 Resulting temperatures near the main cutting edge (left) and average temperature of the main cutting edge (right) at a volume flow rate of 1 l/min.

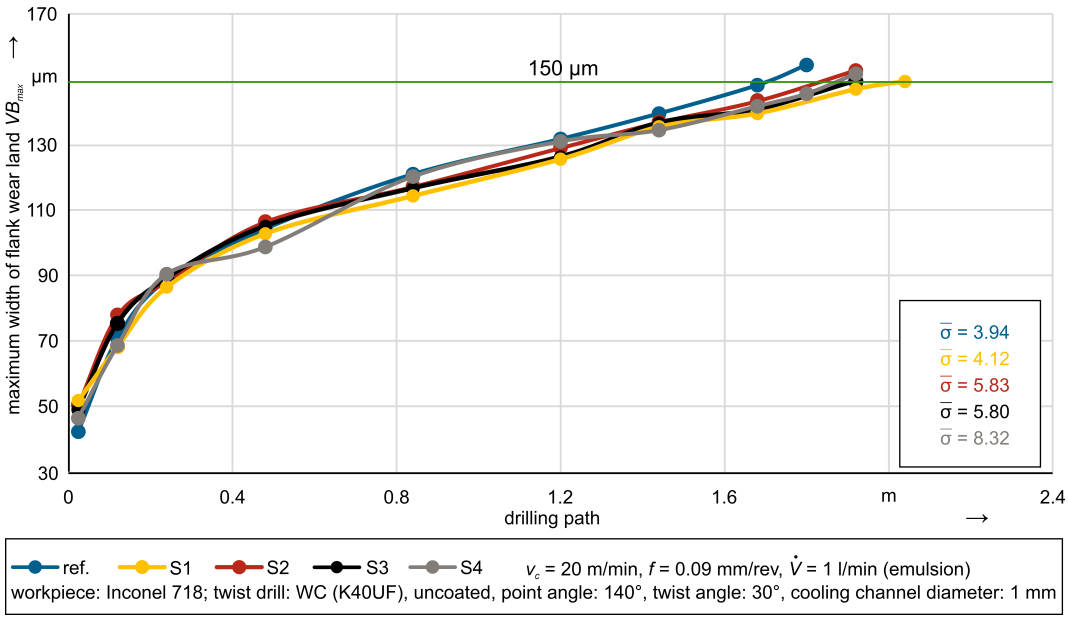

Figure 11 Maximum width of flank wear land (VB_{max}) depending on the structuring of the drills.

Figure 13 shows the surface roughness R_z and R_{max} of the borehole wall depending on the wear condition and structuring.

In the case of the structured drills, the graphs reveal that the surface roughness (R_z and R_{max}) of the borehole wall increases with increasing wear. The reference tool shows no differences for both wear conditions. The structured tools tend to provide a better surface roughness compared to the reference in unworn condition. S1 shows the smallest differences in surface roughness compared to the reference. Without wear, R_z and R_{max} are reduced by approx. 1 µm compared to the reference, at $VB_{max} = 150$ µm there are no differences. S2 has the lowest values for R_z and R_{max} at $VB_{max} = 0$ µm, but the values are about 1 µm

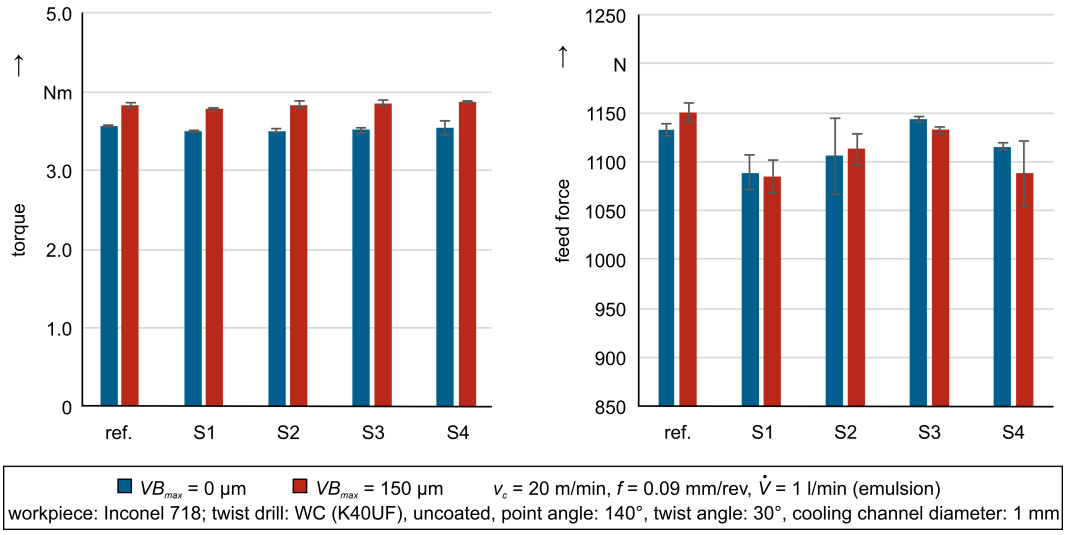

Figure 12 Measured torques in the rotational axis and forces in feed direction depending on the wear condition and structuring.

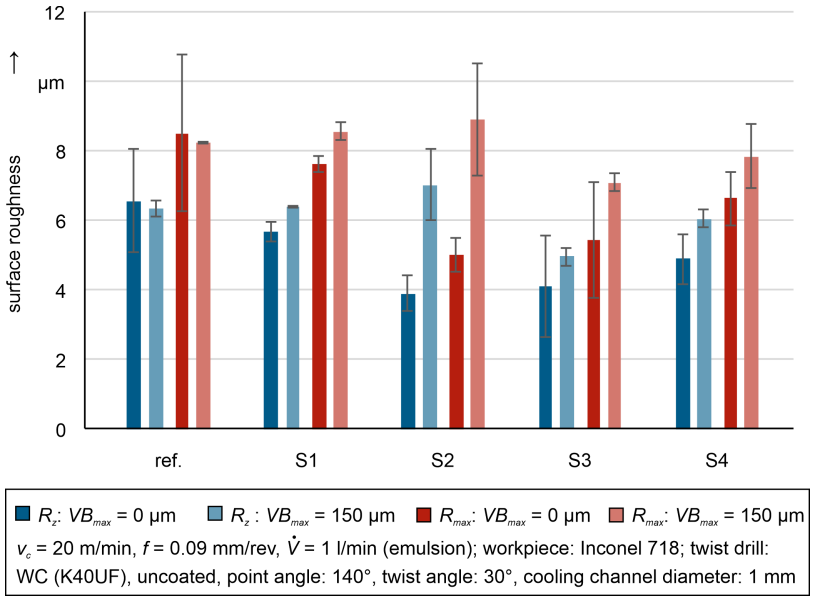

Figure 13 Measured torques in the rotational axis and forces in feed direction depending on the wear condition and structuring.

above the reference values in the worn state. For both wear conditions, S3 shows reduced surface roughness values (R_z and R_{max}) compared to the reference. Without wear, the values forR_z are about 2.5 µm below the values of the reference, at $VB_{max} = 150$ µm about 1.5 µm. In comparison with the reference, S4 has lower R_z and R_{max} values for both wear conditions. The differences are within a maximum range of 1.5 µm.

The borehole quality, determined by the evaluation of the roundness, concentricity and the borehole diameter, depending on wear as well as the structuring, is shown in Figure 14.

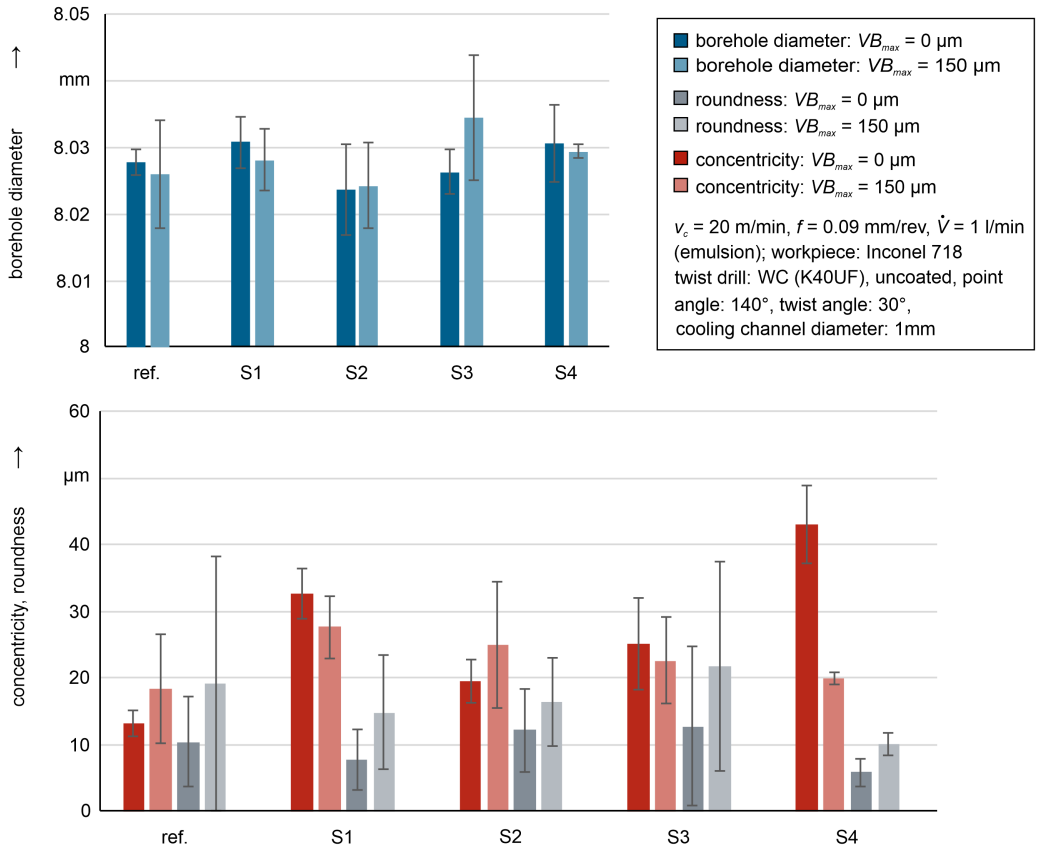

Figure 14 Measured torques in the rotational axis and forces in feed direction depending on the wear condition and structuring.

The measurements do not reveal any significant or systematic influence of the structuring and wear in terms of the diameter of the boreholes. The roundness values tend to increase with increasing wear. S4 shows an improved borehole roundness compared to the reference and other structured drills. The deviation in concentricity of S4, on the other hand, is significantly increased compared to the other drills for the unworn condition. At $VB_{max} = 150$ µm, however, the concentricity does not significantly differ from those of the other drill variants.

5 Conclusion and Outlook

In this paper the influence of different structured flank faces on cooling efficiency, tool life, process forces and borehole quality were investigated. For this purpose, the work was divided into a simulative and an experimental part. The aim of the simulative investigations was to analyze the influence of structures in the area of the first flank face on the flow conditions and thus the cooling of the drills. By means of the experimental investigations the interactions between optimized flow conditions and the tool life as well as the borehole quality could be investigated. The following conclusions can be drawn from the investigations:

The unstructured tool displays low flow velocities and larger dead zones in the area of the cutting edge. As a result, the cutting edge is not sufficiently cooled and is therefore exposed to high thermal loads. By integrating structures near the main cutting edge, the

flow conditions in this area could be improved. In particular a grooved structure along the main cutting edge reduces dead zones in this area and near to the cutting edge corner. As a result, the cooling is improved and the temperatures in the cutting wedge, especially near the thermally high loaded cutting edge corner could be reduced.

The results of the simulations show a good accordance with the conducted tool life tests. A correlation between simulated thermal load of the tools and the achieved tool life was shown. Compared to the non-structured drills, significant increases in tool life of up to 21 % have been achieved through the structuring. Since the same process conditions (feed rate, cutting speed, MWF-flow rate and pressure) and the same drill geometry were used for all investigated drills, these longer tool lifetimes can be attributed to the improved flow conditions resulting from the structuring.

The examined structures have no influence on the process forces. The observed differences in borehole quality should not be regarded as insignificant, as the functionality of the boreholes is not affected by any of the modifications.

In further studies, the influence of the structure depth and the distance to the main cutting edge will be investigated. In addition, the influence of the cooling channel design on the flow conditions of the MWF in the borehole will be investigated through visualization investigations using particle tracking.

[1] Naming of specific manufacturers is done solely for the sake of completeness and does not necessarily imply an endorsement of the named companies nor that the products are necessarily the best for the purpose.

References

1 Y. Altintas. *Manufacturing automation: metal cutting mechanics, machine tool vibrations, and CNC design*. Cambridge University Press, 2012.

2 Ansys. Cfx - pre user's guide, 2011.

3 N. Beer, E. Oezkaya, and D. Biermann. Drilling of inconel 718 with geometry-modified twist drills. *Procedia Cirp*, 24:49–55, 2014. doi:10.1016/j.procir.2014.07.124.

4 I.A. Choudhury and M.A. El-Baradie. Machinability of nickel-base super alloys: a general review. *Journal of Materials Processing Technology*, 77(1-3):278–284, 1998. doi:10.1016/S0924-0136(97)00429-9.

5 F. Fallenstein and J.C. Aurich. Cfd based investigation on internal cooling of twist drills. *Procedia CIRP*, 14:293–298, 2014. doi:10.1016/j.procir.2014.03.112.

6 F. Fallenstein and J.C. Aurich. Kühlkanalaustrittsbedingungen beim bohren. *wt Werkstattstechnik online*, 105:495–500, 2015.

7 D. Guo, X. Guo, K. Zhang, Y. Chen, C. Zhou, and L. Gai. Improving cutting performance of carbide twist drill combined internal cooling and micro-groove textures in high-speed drilling ti6al4v. *The International Journal of Advanced Manufacturing Technology*, 100(1-4):381–389, 2018. doi:10.1007/s00170-018-2733-z.

8 C. Hirsch. *Numerical computation of internal and external flows: The fundamentals of computational fluid dynamics*. Elsevier, 2007. doi:10.1016/B978-0-7506-6594-0.X5037-1.

9 P. Hänle and M. Schwenck. Optimization of cutting tools using ca-technologies. *International Workshop on Modeling of Machining Operations*, 8:463–468, 2005.

10 F. Klocke. *Manufacturing Processes 1*. Springer-Verlag Berlin Heidelberg, 2011.

11 I. Lazoglu, G. Poulachon, C. Ramirez, M. Akmal, B. Marcon, F. Rossi, J.C. Outeiro, and M. Krebs. Thermal analysis in ti-6al-4v drilling. *CIRP Annals*, 66(1):105–108, 2017.

12 D. Mueller, B. Kirsch, and J.C. Aurich. The influence of structured flank faces on cooling performance when drilling. *Procedia CIRP*, 82:415–420, 2019. doi:10.1016/j.procir.2019.03.274.

13 D. Mueller, B. Kirsch, and J.C. Aurich. Kühlkanalaustrittsbedingungen bei bohrern. *wt Werkstattstechnik online*, 109(1/2):30–34, 2019.

14 D. Mueller, A. Lange, B. Kirsch, and J.C. Aurich. Kühlkanalaustrittsbedingungen beim bohren. *ZWF*, 113:471–474, 2018.

15 E. Oezkaya, N. Beer, and D. Biermann. Experimental studies and cfd simulation of the internal cooling conditions when drilling inconel 718. *International Journal of Machine Tools and Manufacture*, 108:52–65, 2016. doi:10.1016/j.ijmachtools.2016.06.003.

16 E. Oezkaya, M. Bücker, and D. Biermann. Simulative analyses focused on the changes in cutting fluid supply of twist drills with a modified flank face geometry. *International Journal of Mechanical Sciences*, 180, 2020. doi:10.1016/j.ijmecsci.2020.105650.

17 E. Oezkaya, I. Iovkov, and D. Biermann. Fluid structure interaction (fsi) modelling of deep hole twist drilling with internal cutting fluid supply. *CIRP Annals*, 68(1):81–84, 2019. doi:10.1016/j.cirp.2019.03.003.

18 J. Rech, P.J. Arrazola, C. Claudin, C. Courbon, F. Pusavec, and J. Kopac. Characterisation of friction and heat partition coefficients at the tool-work material interface in cutting. *CIRP Annals*, 62(1):79–82, 2013. doi:10.1016/j.cirp.2013.03.099.

19 S. Rodriguez. *Applied Computational Fluid Dynamics and Turbulence Modeling*. Springer, 2019.

20 H.K. Toenshoff and B. Denkena. *Basics of cutting and abrasive processes*. Springer-Verlag Berlin Heidelberg, 2013. doi:10.1007/978-3-642-33257-9.

21 D. Zhu, X. Zhang, and H. Ding. Tool wear characteristics in machining of nickel-based superalloys. *International Journal of Machine Tools and Manufacture*, 64:60–77, 2013. doi:10.1016/j.ijmachtools.2012.08.001.